Research Article

# Efficient photocatalytic hydrogen production by $Zn_{(1-2x)}Cu_xIn_2S_{(4-1.5x)}$ co-doped with Cu and excess in under visible light irradiation

Ikki Tateishi[1] · Mai Furukawa[2] · Hideyuki Katsumata[2] · Satoshi Kaneco[1,2]

Received: 10 June 2020 / Accepted: 27 August 2020 / Published online: 12 September 2020


**Abstract**
Herein, in order to achieve visible light responsive ability and efficient photogenerated electron–hole pairs separation $Zn_{(1-2x)}Cu_xIn_2S_{(4-1.5x)}$ photocatalysts were fabricated through a simple one-step solvothermal method. The effects of the Cu/Zn molar ratios on the crystal structure, morphology, optical property, as well as photocatalytic activity have been investigated in detail. In addition, the stability of the photocatalysts and apparent quantum yield were measured. The band gap became wider due to the decrease in Cu doping and Zn. The band gap of $Zn_{(1-2x)}Cu_xIn_2S_{(4-1.5x)}$ ($x = 0 \sim 0.20$) decreased from 2.67 to 1.76 eV with the increase in x value. When Pt was used as a co-catalyst, $H_2$ evolution rates up to 2400 μmol $g^{-1}$ $h^{-1}$ were achieved over $Zn_{0.74}Cu_{0.13}In_2S_{3.805}$. Furthermore, when PdS was used as a co-catalyst, the hydrogen generation rates were improved with up to 3600 μmol $g^{-1}$ $h^{-1}$ by optimizing the $Zn_{(1-2x)}Cu_xIn_2S_{(4-1.5x)}$. The apparent quantum yield achieved 16% at 420 nm, 9.4% at 500 nm and 9.1% at 600 nm when $x = 0.20$. The improved visible light photocatalytic performance is considered to be due to the manipulation of the band structure and efficient photogenerated charge separation due to the effects of Cu doping and composition ratio.

**Keywords** Photocatalysis · $ZnIn_2S_4$ · Photocatalytic hydrogen evolution · Visible light · $CuInS_2$ · $In_2S_3$

## 1 Introduction

Metal sulfide photocatalysts compared to the metal oxide photocatalysts have a advantageous band structure for photocatalytic hydrogen evolution under visible light [1–6]. Among the various metal sulfide photocatalysts, the ternary metal chalcogenide $ZnIn_2S_4$ may be superior to other sulfides due to low toxicity, good absorption of visible light and stability during photocatalysis [7–10]. However, pure $ZnIn_2S_4$ has limited enhancement of photocatalytic hydrogen production under visible light due to high recombination rate of photogenerated electron–hole pairs and optical absorption range of about $\lambda < 500$ nm [11, 12]. In order to solve these drawbacks and enhance the photocatalytic hydrogen production ability, heterojunction strategies between various materials and $ZnIn_2S_4$ and metal doping to $ZnIn_2S_4$ were investigated. [13–17]. Yang and co-researchers have reported Cu and Ga co-doped $ZnIn_2S_4$ for enhanced photocatalytic hydrogen generation activity [17]. $CuInS_2$ is a ternary chalcogenide semiconductor with a band gap and high absorption coefficient that is well matched to the AM0 or AM1.5 solar spectrum. Therefore, combination with $CuInS_2$ and $ZnIn_2S_4$ was investigated and a high hydrogen generation capacity was revealed [18–20]. In particular, the lattice between $CuInS_2$ and $ZnIn_2S_4$ is better matched by similar sulfides compared to other coupled photocatalysts [21]. Indium sulfide ($In_2S_3$) is expected as candidate for optoelectronic and photovoltaic materials because of

**Electronic supplementary material** The online version of this article (https://doi.org/10.1007/s42452-020-03450-2) contains supplementary material, which is available to authorized users.

✉ Ikki Tateishi, tateishi@gecer.mie-u.ac.jp | [1]Mie Global Environment Center for Education and Research, Tsu, Mie 514-8507, Japan. [2]Department of Chemistry for Materials, Graduate School of Engineering, Mie University, Tsu, Mie 514-8507, Japan.

its low toxicity, high carrier mobility and stability in photocatalytic reactions [22, 23]. Song et al. showed improved hydrogen-producing activity of $ZnIn_2S_4/In_2S_3$ prepared by CTAB-assisted hydrothermal method with excess indium and found optimum content of indium [23]. It is generally reported that an excess or deficiency of the doping amount is disadvantageous to the photocatalytic activity [13, 14, 17]. Therefore, investigation of the optimal doping amount is necessary for further improvement of photocatalytic activity. In this study, adjustment of the composition ratio and co-catalyst was investigated to further improve the photocatalytic activity of a series of $Zn_{(1-2x)}Cu_xIn_2S_{(4-1.5x)}$ ($x$=0, 0.03, 0.06, 0.10, 0.13, 0.20) photocatalysts doped with different amounts of Cu and excess In.

## 2 Experiment

### 2.1 Preparation of photocatalysts

In this experiment, all chemicals were of analytical purity and used without further purification. The $Zn_{(1-2x)}Cu_xIn_2S_{(4-1.5x)}$ ($x$=0, 0.01, 0.03, 0.06, 0.10, 0.13, 0.20) photocatalysts were prepared by previous reported CTAB-assisted one-step hydrothermal method [24]. Cetyltrimethylammonium bromide (CTAB, 3.76 mmol) (Wako Pure Chemical Industries, Osaka, Japan), stoichiometric moles of $ZnSO_4$ $7H_2O$ (Nacalai Tesque, Kyoto, Japan), $InCl_3{\cdot}4H_2O$, CuCl (I) and excess thioacetamide (TAA, 8.00 mmol) (Wako Pure Chemical Industries, Ltd., Osaka, Japan) were dissolved in 50 mL of distilled water under stirring. Then, to remove dissolved oxygen and keep the added Cu monovalent, the mixture solution was purged with nitrogen for 10 min. The mixture was added into a 100 mL Teflon autoclave. The autoclave was sealed and held at 160 °C for 1 h and naturally cooled to room temperature. After cooling, the products were washed with ethanol and distilled water few times, respectively, then vacuum-dried at 40 °C for 4 h and ground for 30 min. $ZnIn_2S_4$ was prepared in the same method as the reference material.

### 2.2 Characterization of samples

Crystalline phases of the photocatalysts were decided from X-ray diffraction (XRD) patterns measured a Rigaku RINT Ultima-IV diffractometer. It was measured by scanning rate of 0.04°/s and employing Cu radiation source. Crystallite size was determined using Scherrer's Eq. (1).

$$D = \frac{K \times \lambda}{B \times \cos\theta} \tag{1}$$

where $D$, $K$, $\lambda$, $B$ and $\theta$ represent crystallite size, the shape factor (0.9), Cu Kα wavelength (0.154056 nm), full width at half maximum intensity in radians and Bragg's diffraction angle, respectively. To determine the binding state of the contained elements and the position of valence band (VBXPS), X-ray photoelectron spectroscopy (XPS) measurements were obtained on a PHI Quantera SXM photoelectron spectrometer using Al Kα radiation source. Elemental mapping of prepared photocatalyst was determined by electron probe microanalysis (EPMA) with JXA-8530F. Binding energy was corrected using the C1s peak at 284 eV as a reference for surface charge effects. Surface condition of samples was observed using scanning electron microscope (SEM) with a Hitachi S-4000. Also, internal structure was observed by the transmission electron microscopy (TEM) on JEOL JEM1011. UV–Vis diffuse reflectance spectra (DRS) were measured using Shimadzu UV-2450 spectrophotometer equipped with an integrating sphere attachment and $BaSO_4$ as a reference standard. Using a Shimadzu RF-5300PC, photoluminescence (PL) spectra of each photocatalyst were detected with an excitation wavelength of 350 nm. To calculate the band gap energy, a classical extrapolation approach was using Eq. (2), and the positions of the valence band and the conduction band were estimated from VBXPS and band gap energy measurement results.

$$\alpha h\nu = A\left(h\nu - E_g\right)^n \tag{2}$$

where $h\nu$, $\alpha$, $A$ and $E_g$ represent the discrete photon energy, optical absorption coefficient, Planck's constant and photonic energy band gap, and $n$ = 1/2 for direct band gap semiconductor [25].

### 2.3 Photocatalytic hydrogen generation experiment

The photocatalytic hydrogen generation experiment was tested in the 123-mL Pyrex reactor. A 300 W xenon lamp was employed as the side irradiation light source equipped with cutoff filter ($\lambda \geq 420$ nm) due to remove UV part. In all experiments, 40 mL (pH 12) of solution containing 40 mg of catalyst, 10 mL of 0.04 ppm co-catalyst solution (1 wt%) and 0.25 M $Na_2SO_3$/0.35 M $Na_2S$ mixed sacrificial agent was added into the reaction cell. The light source was a 4000–4500 μW/cm$^2$ Xe lamp for 6 h, with a cutoff filter ($\lambda \geq 420$ nm). The co-catalysts were loaded onto the photocatalyst by dropping a 1000 ppm standard solution into the reaction vessel and irradiating with visible light. Nitrogen purged through the system for 30 min before reaction to remove oxygen. The concentrations of $H_2$ were measured using gas chromatograph system (GC) consisting of injection, column and thermal conductivity detector (TCD), of which temperatures were kept at 50 °C. The hydrogen generation experimental conditions are shown in Table 1. On the stability of the photocatalyst,

one cycle of photocatalytic hydrogen generation was 6 h, and 4 cycles were performed under the same conditions. At the end of each cycle, a nitrogen purge was performed in the reaction vessel to remove residual hydrogen. Apparent quantum yield was measured using band-pass filter (420 nm, 500 nm and 600 nm) and calculated using Eq. (3).

$$\text{A.Q.Y.}(\%) = \frac{\text{Number of reacted electrons}}{\text{Number of incident electrons}} \times 100 = \frac{\text{Number of evolved } H_2 \text{ molecules} \times 2}{\text{Number of incident photons}} \times 100 \quad (3)$$

## 3 Results and discussion

### 3.1 Photocatalytic activity

For optimal co-catalyst studies, Rh, Ru, Pt, or PdS was loaded on $Zn_{0.74}Cu_{0.13}In_2S_{3.905}$ and compared hydrogen generation rates. The result is shown in Fig. S1. The hydrogen production activity of the photocatalyst loaded with each co-catalyst improved in the order of Rh < Ru < Pt < PdS.

Figure 1 shows the effect of Cu and excess In doping amount was studied with $Zn_{(1-2x)}Cu_xIn_2S_{(4-1.5x)}$ ($x = 0$, 0.01, 0.03, 0.06, 0.10, 0.13 and 0.20). The hydrogen production activity of each $Zn_{(1-2x)}Cu_xIn_2S_{(4-1.5x)}$ catalyst was great in the order of $x = 0 < x = 0.01 < x = 0.13 < x = 0.20 < x = 0.10 < x = 0.06 < x = 0.03$. The hydrogen generation rate of $Zn_{0.94}Cu_{0.03}In_2S_{3.955}$ was the highest, reaching about 3600 μmol $g^{-1}$ $h^{-1}$. This result is about four times as high as 900 μmol $g^{-1}$ $h^{-1}$ of the hydrogen production rate of pure $ZnIn_2S_4$ using PdS as co-catalyst. This difference in hydrogen generation activity is considered to be due to the increase in absorption wavelength due to the incorporation of $CuInS_2$ and $In_2S_3$ into $ZnIn_2S_4$. Thus, the higher hydrogen generation rate of $x = 0.03$ than $x = 0$ is largely related to the absorption of light with a wavelength of 400 nm to 600 nm from result of DRS. Photocatalytic $H_2$ production of recent works on metal chalcogenide photocatalysts is given in Table S1.

**Table 1** Hydrogen generation experimental conditions

| | |
|---|---|
| Photocatalyst | $Zn_{(1-2x)}Cu_xIn_2S_{(4-1.5x)}$ ($x = 0$, 0.01, 0.03, 0.06, 0.10, 0.13 and 0.20) |
| Co-catalyst | Pt, PdS, Ru or Rh 0.04 mg (1.0 wt%) |
| Medium | 0.25 M $Na_2SO_3$/0.35 M $Na_2S$ 40 mL, pH12 |
| Reactor | Pyrex glass vessel (volume: 123 mL) |
| Temperature | Room temperature (25 °C) |
| Light source | Xenon lamp ($\lambda \geqq 420$ nm, 4500 μW/$cm^2$) |
| Irradiation time | 6 h |
| Analysis | Gas chromatography (TCD) |

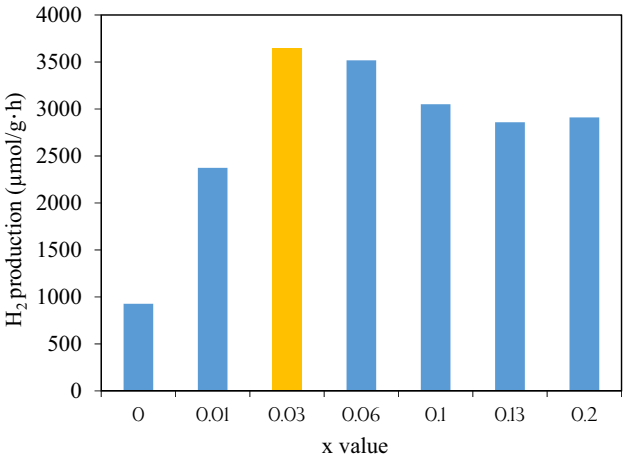


**Fig. 1** Photocatalytic hydrogen production rate with $Zn_{(1-2x)}Cu_xIn_2S_{(4-1.5x)}$

The stability of the photocatalytic activity is also important to obtain a stable amount of hydrogen production. In order to research stability, $Zn_{0.94}Cu_{0.03}In_2S_{3.955}$ loaded PdS 1.0 wt% under visible light irradiation was performed in a time-dependent photocatalytic hydrogen production cycle experiment, as shown in Fig. 2. The hydrogen generation activity of $Zn_{0.94}Cu_{0.03}In_2S_{3.955}$ did not decrease significantly in the second cycle. However, after the third cycles, the catalytic activity of hydrogen production decreased to some extent. This phenomenon may have resulted in slight deterioration of the photocatalyst, because of the long-time photocatalytic hydrogen production reaction process.

As we investigate the cause of enhanced photocatalytic ability, the apparent quantum yield in the visible region

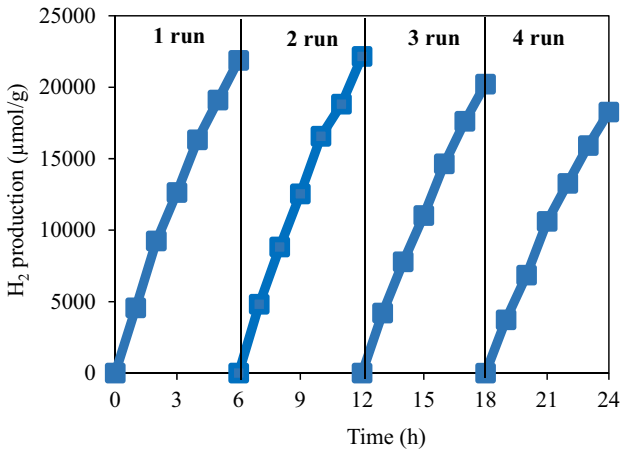


**Fig. 2** Cycling runs of $Zn_{0.94}Cu_{0.03}In_2S_{3.955}$

was investigated. Table S2 shows an apparent quantum yield when a xenon lamp irradiated to a $Zn_{0.94}Cu_{0.03}In_2S_{3.955}$ and $Zn_{0.60}Cu_{0.20}In_2S_{3.70}$ photocatalysts through a band-pass filter which passes wavelengths of only 420 nm, 500 nm and 600 nm. The apparent quantum yield was higher at $Zn_{0.94}Cu_{0.03}In_2S_{3.955}$ than at $Zn_{0.60}Cu_{0.20}In_2S_{3.70}$ in the short wavelength ($\lambda = 420$ nm and 500 nm). Conversely, in the long wavelength ($\lambda = 600$ nm), the apparent quantum yield showed a higher at $Zn_{0.60}Cu_{0.20}In_2S_{3.70}$. These result were consistent with the measurement results of DRS and suggest that the improvement of the hydrogen production activity of $Zn_{(1-2x)}Cu_xIn_2S_{(4-1.5x)}$ photocatalyst is mainly due to the light absorption ability.

### 3.2 Structural characterization

Figure 3 shows XRD pattern measurements of prepared $ZnIn_2S_4$, $Zn_{0.94}Cu_{0.03}In_2S_{3.955}$, $Zn_{0.74}Cu_{0.13}In_2S_{3.805}$ and $Zn_{0.60}Cu_{0.20}In_2S_{3.7}$. The XRD pattern of $ZnIn_2S_4$, $Zn_{0.94}Cu_{0.03}In_2S_{3.955}$, $Zn_{0.74}Cu_{0.13}In_2S_{3.805}$ and $Zn_{0.60}Cu_{0.20}In_2S_{3.7}$ can be indexed as a hexagonal $ZnIn_2S_4$ structure (JCPDS No. 65-2023). These XRD patterns are consistent with those reported in previous studies [26], and $Zn_{(1-2x)}$ $Cu_xIn_2S_{(4-1.5x)}$ has a hexagonal structure regardless of the amount of doping and is similar to ZnS. It became clear that it contained almost no impurities. No peaks derived from Cu and excess In were observed. This is due to a very small amount of doping. Furthermore, with respect to the (006) plane peak, Cu doping and excess In cause a slight shift to high angles. This means that the planar spacing has been reduced by doping, suggesting that Cu and excess In may be incorporated into the $ZnIn_2S_4$ crystal structure and exist as a solid solution. The crystallite sizes calculated using Scherrer's equation are listed in Table S3. Crystallite size decreased slightly with increasing Cu and excess In doping.

In order to confirm Cu and Pd element, the $Zn_{0.60}Cu_{0.20}In_2S_{3.7}$ was research by XPS. The results are shown in Fig. 4. Also, Table S4 shows the element ratios of each photocatalytic catalyst determined from the XPS spectrum. Figure S2 shows the survey spectra before and after the hydrogen production are almost same. In the narrow spectrum, Zn 2p spectrum shows two peaks at the binding energies of 1020.4 eV and 1043.6 eV. The two peaks are indexed $Zn2p_{3/2}$ and Zn $2p_{1/2}$, respectively. The positions of peaks at 452.7 eV and 445.1 eV can be belonging to In $2p_{3/2}$ and In $2p_{5/2}$, and the positions of peaks at 161.3 eV and 162.6 eV peaks for S 2p are indexed at S $2p_{3/2}$ and S $2p_{1/2}$, which attribute to $ZnIn_2S_4$, $In_2S_3$ and $CuInS_2$, respectively. Cu $2p_{3/2}$ peaks positioned at 932 eV indicate that Cu is monovalent, and the presence of $CuInS_2$ [27, 28]. Also, Pd peak is not observed before the hydrogen production experiment, but after the experiment Pd presence can be confirmed. This XPS result indicates that Pd employed was deposited as PdS on the catalyst. Furthermore, elemental mapping using EPMA measurements showed that Zn, In, S and Cu were uniformly present in the photocatalyst particles (Fig. S3).

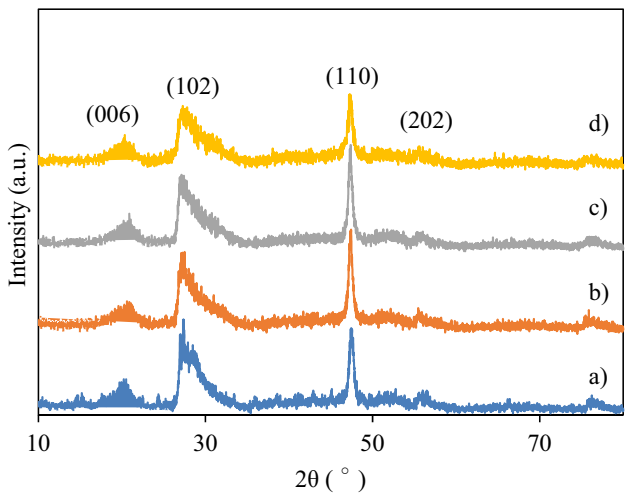


**Fig. 3** XRD pattern of a $ZnIn_2S_4$, b $Zn_{0.94}Cu_{0.03}In_2S_{3.955}$, c $Zn_{0.74}Cu_{0.13}In_2S_{3.805}$ and d $Zn_{0.60}Cu_{0.20}In_2S_{3.7}$

### 3.3 Morphological analysis

The morphology of as-synthesized $Zn_{(1-2x)}Cu_xIn_2S_{(1-1.5x)}$ ($x = 0$, 0.03, 0.06, 0.10, 0.13, 0.20) photocatalyst was characterized by SEM and TEM. Figure 5a shows the typical petal-microsphere $ZnIn_2S_4$ with folding the nanosheet [24, 30]. Figures 5b and 4c show increasing the doping amount of Cu and excess In broke the spherical structure. The nanosheet structure is obvious up to $x = 0.06$. However, when values of x higher than that, the nanosheet structure was agglomerated. The difference of morphology between $x = 0$ with $x = 0.10$, 0.13 and 0.20 was clear. It suggests that the solid solution was formed by doping Cu and excess In. The TEM images of prepared $Zn_{(1-2x)}Cu_xIn_2S_{(4-1.5x)}$ photocatalysts are shown in Fig. S4. At $ZnIn_2S_4$, several thin lines were observed. It suggests a petal-microsphere structure with nanosheets. When $x = 0.03$ and 0.06, microsphere was not observed and nanosheets were reduced clearly. When $x = 0.10$, 0.13 and 0.20, the nanosheets were almost unobservable and almost no transmission. This result suggests doping Cu and excess In broke morphology. It matched the SEM images. The mechanism of change shape is still unclear at present and requires further researches.

### 3.4 Optical analysis

The effects of Cu and excess In doping amount to the absorption region in $Zn_{(1-2x)}Cu_xIn_2S_{(4-1.5x)}$ ($x = 0$, 0.03, 0.06,

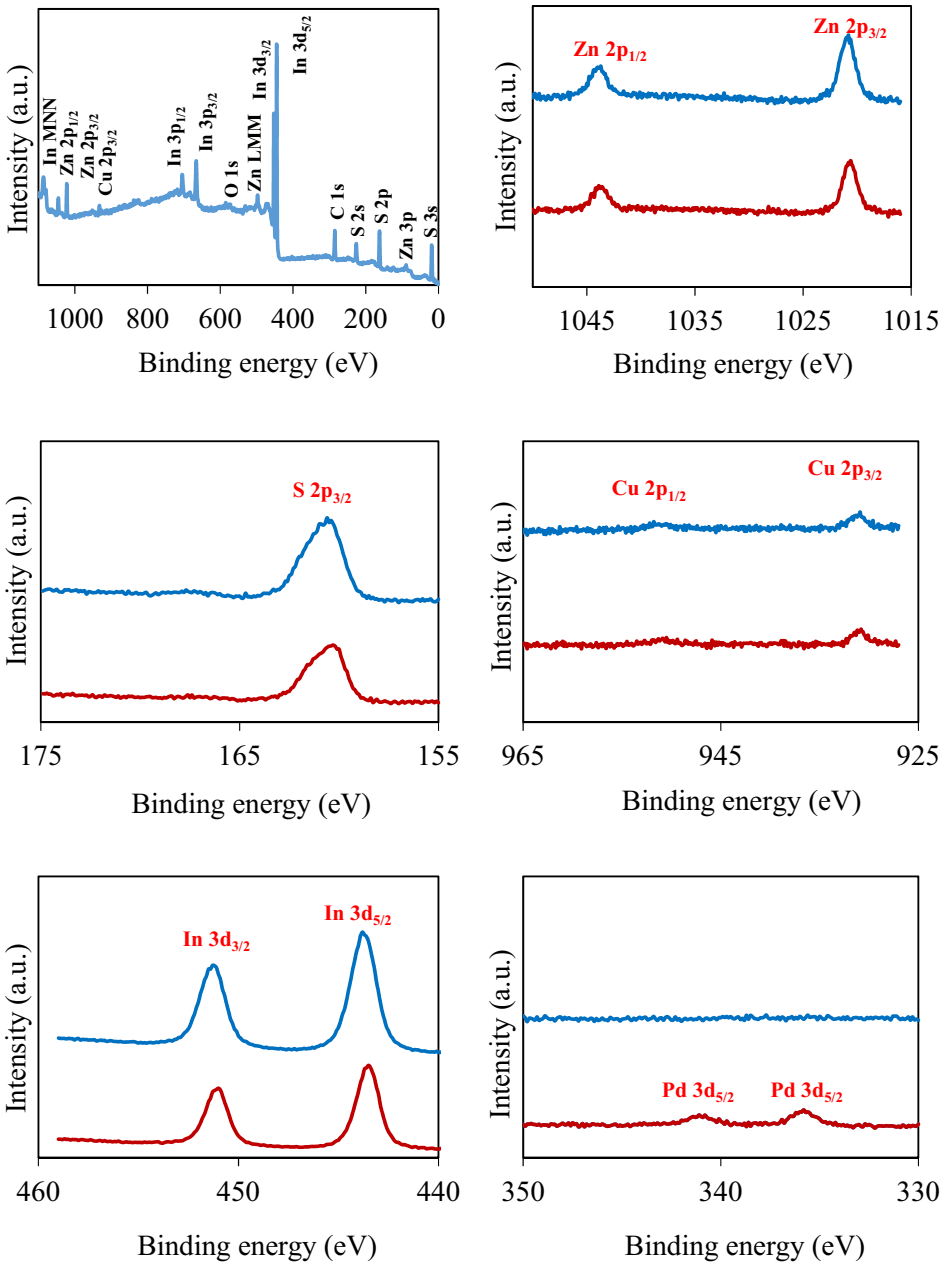


**Fig. 4** XPS narrow and survey spectra of $Zn_{0.60}Cu_{0.20}In_2S_{3.7}$, before hydrogen production and after hydrogen production. Blue line: before, red line: after

0.10, 0.13 and 0.20) were investigated by UV–Vis diffuse reflectance spectra (DRS) in Fig. 6. Tauc plot obtained from the UV–Vis DRS spectrum for estimating band gap energy is shown in Fig. S5.

As shown in the results of DRS and Tauc plot, the absorption edge of $ZnIn_2S_4$ without doping was the shortest of the other samples, less than 500 nm, and the calculated the band gap energy was about 2.67 eV. On the other hand, the absorption edge of the excess In- and Cu-doped $Zn_{(1-2x)}Cu_xIn_2S_{(4-1.5x)}$ photocatalysts had more red-shift with an increase in the doping amount. The absorption edge of $Zn_{0.60}Cu_{0.20}In_2S_{3.7}$ reached up to 770 nm. The absorbance of the $Zn_{(1-2x)}Cu_xIn_2S_{(4-1.5x)}$ ($x = 0.03$ and 0.06) photocatalysts was higher than that of the $Zn_{(1-2x)}Cu_xIn_2S_{(4-1.5x)}$ ($x = 0.10$, 0.13 and 0.20) at wavelengths of less than 550 nm. As well, the band gap energy decreased as the amount of excess In and Cu doping increasing. The band gap energy of $Zn_{0.60}Cu_{0.20}In_2S_{3.7}$ photocatalyst decreases up to 1.98 eV.

In order to further research the band structure of photocatalyst, valence band edge was measured for the prepared photocatalysts by XPS. Figure S6 shows that the doping of Cu and excess In shifted the valence band edge to the negative side. This result was consistent with previous studies which show that $Cu^+$ doping inserts Cu 3d orbital into the $ZnIn_2S_4$ valence band and shifts it to the

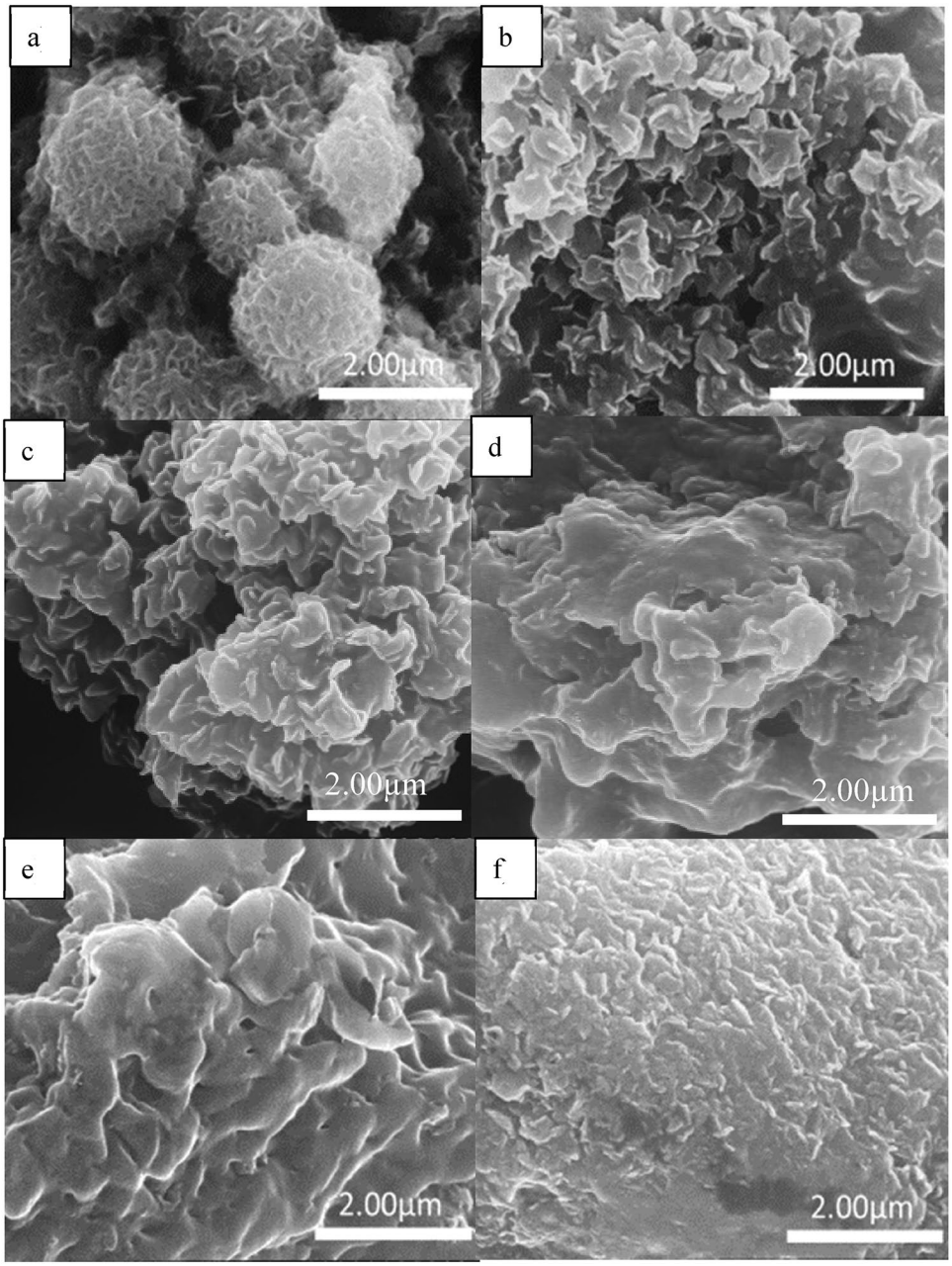


**Fig. 5** SEM images of $Zn_{(1-2x)}Cu_xIn_2S_{(4-1.5x)}$. **a** $x=0$, **b** $x=0.03$, **c** $x=0.06$, **d** $x=0.10$, **e** $x=0.13$ and **f** $x=0.20$ (**a** from reproduction of Fig. 3 in Ref. [29])

negative side [12, 22]. The significant decrease in band gap energy size compared to the valence band shift level indicates that the conduction band is positively shifted. The conduction band shifting effect is due to excess In doping. It was reported that the inserting of $In^{3+}$ constitutes a sub-band on the positive side than the conduction band of $ZnIn_2S_4$ [31].

Photoluminescence spectrum was recorded for $ZnIn_2S_4$, $Zn_{0.94}Cu_{0.03}In_2S_{3.955}$, $Zn_{0.74}Cu_{0.13}In_2S_{3.805}$ and $Zn_{0.60}Cu_{0.20}In_2S_{0.37}$ due to investigate the effect of the doping amount of Cu and excess indium to the recombination of photogenerated electron/hole pairs in photocatalyst. Generally, the stronger PL intensity suggests the high recombination rate of photogenerated carriers. And as shown in Fig. 7, pure $ZnIn_2S_4$ has a broad emission peak of 400–700 nm, which represents multiple recombination centers [32, 33]. The peak intensity of $Zn_{0.94}Cu_{0.03}In_2S_{3.955}$ decreased dramatically compared to $ZnIn_2S_4$, and that of $Zn_{0.74}Cu_{0.13}In_2S_{3.805}$ further decreased. However, intensity of $Zn_{0.60}Cu_{0.20}In_2S_{0.37}$ increased dramatically compared to $Zn_{0.74}Cu_{0.13}In_2S_{3.805}$. This phenomenon is consistent with the results that reported [26]. This suggests that low Cu

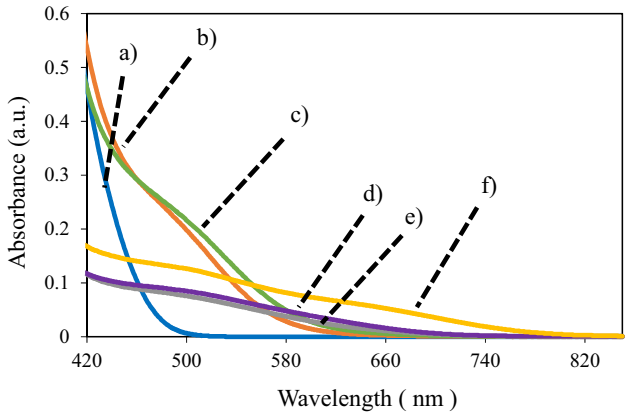


**Fig. 6** UV–Vis spectra of a $ZnIn_2S_4$, b $Zn_{0.94}Cu_{0.03}In_2S_{3.955}$, c $Zn_{0.88}Cu_{0.06}In_2S_{3.91}$, d $Zn_{0.80}Cu_{0.10}In_2S_{3.85}$, e $Zn_{0.74}Cu_{0.13}In_2S_{3.805}$ and f $Zn_{0.60}Cu_{0.20}In_2S_{0.37}$

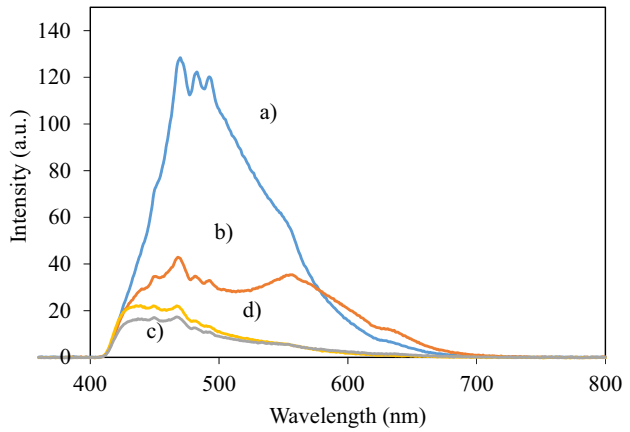


**Fig. 7** Photoluminescence spectra for $Zn_{(1-2x)}Cu_xIn_2S_{(4-1.5x)}$. a $ZnIn_2S_4$, b $Zn_{0.94}Cu_{0.03}In_2S_{3.955}$, c $Zn_{0.74}Cu_{0.13}In_2S_{3.805}$ and d $Zn_{0.60}Cu_{0.20}In_2S_{0.37}$. Excitation: 350 nm

and excessive In doping can effectively delay the recombination of electron/hole pairs, but high doping promotes recombination.

### 3.5 Proposed hydrogenation mechanism

The reaction mechanism based on the band gap of $Zn_{0.94}Cu_{0.03}In_2S_{3.955}$ loaded PdS 1.0 wt% is shown in Fig. 8. The valence band edge of pure $ZnIn_2S_4$ is composed of S3p + Zn3d, and the conduction band edge is composed of In5s5p + Zn4s4p [17]. Regarding the conduction band of $Zn_{(1-2x)}Cu_xIn_2S_{(4-1.5x)}$, the ratio of $In_2S_3$ increases by lowering the ratio of Zn in $ZnIn_2S_4$, and the effect of the In5s5p electron orbit derived from $In_2S_3$ becomes large, so the conduction band is considered to shift to the positive position. The valence band of $Zn_{(1-2x)}Cu_xIn_2S_{(4-1.5x)}$ is considered to be that, by doping Cu into $ZnIn_2S_4$, Cu3d is added to S3p + Zn3d, and the valence band shifts to the negative position. Figure S7 shows the $Zn_{(1-2x)}Cu_xIn_2S_{(4-1.5x)}$ ($x = 0$, 0.03, 0.06, 0.10, 0.20) band structure considered from the valence band edge determined by XPS and the band gap energy determined from DRS. The doping of Cu and excess In has the advantage of enables reaction under longer wavelength light, delaying the recombination of photogenerated electron–hole pairs. On the other hand, high doping amount promotes recombination of photogenerated electron–hole pairs. In addition, excess In doping has the disadvantage of lowering the CB potential and lowering the excess potential for water splitting [26]. Therefore, $Zn_{0.94}Cu_{0.03}In_2S_{3.955}$ was suggested experimentally the best catalyst with a balance between these two factors.

## 4 Conclusion

The $Zn_{(1-2x)}Cu_xIn_2S_{(4-1.5x)}$ photocatalyst was synthesized in situ by a one-pot solvothermal reaction. The $Zn_{(1-2x)}Cu_xIn_2S_{(4-1.5x)}$ photocatalyst significantly improves the photocatalytic performance of $ZnIn_2S_4$ for $H_2$ evolution under visible light illumination.

The $Zn_{(1-2x)}Cu_xIn_2S_{(4-1.5x)}$ photocatalyst is considered to be composed of a $ZnIn_2S_4$-$CuInS_2$-$In_2S_3$ composite catalysts from the XPS results. In addition, $ZnIn_2S_4$, $CuInS_2$ and $In_2S_3$ may be partially in solid solution from XRD results, elemental mapping using EPMA and SEM images.

The $Zn_{(1-2x)}Cu_xIn_2S_{(4-1.5x)}$ heterostructure photocatalyst extends the light absorption wavelength range of $ZnIn_2S_4$ and significantly improves the photocatalytic performance for $H_2$ generation under visible light illumination. The hydrogen generation activity was improved to 3600 μmol $g^{-1}$ $h^{-1}$ with the optimum $Zn_{(1-2x)}Cu_xIn_2S_{(4-1.5x)}$ system. On the other hand, the apparent quantum yield reached up to 9.1% at a wavelength of 600 nm. The doping of Cu and excess In caused the manipulation of the band structure and the hole electron recombination, which contributed to the photocatalytic activity. These results suggest inspiration for the design of composite photocatalysts with visible and efficient photocatalyst $H_2$ generation.

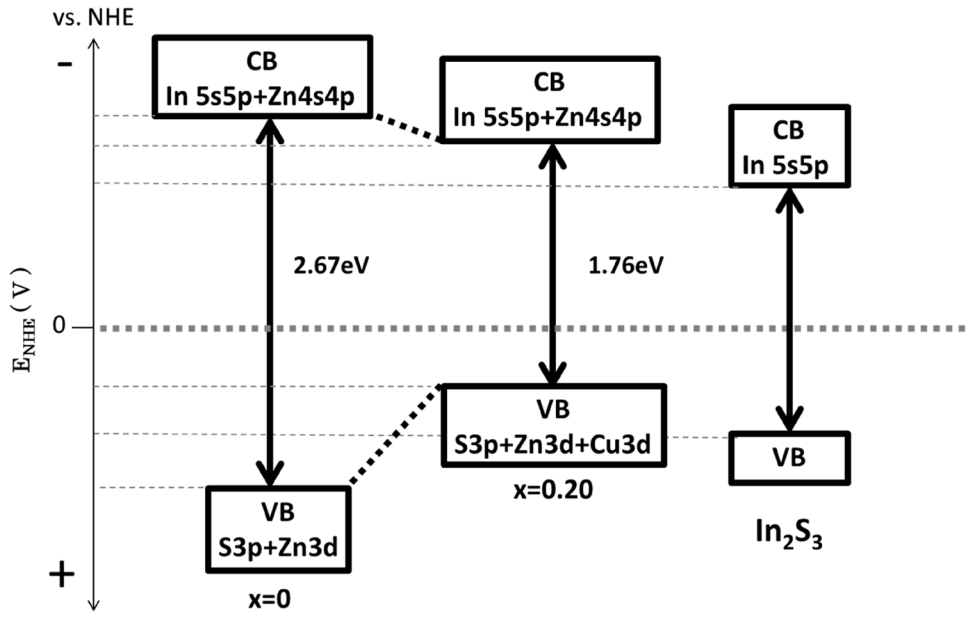


**Fig. 8** Mechanism of band gap with $Zn_{(1-2x)}Cu_xIn_2S_{(4-1.5x)}$ ($x = 0$ and 0.20)

**Acknowledgements** The author is grateful to the graduate school department of Mie University for the financial and technical support of this work.

## Compliance with ethical standards

**Conflicts of interest** The authors declare no conflict of interest.

## References

1. Tsuji I, Kato H, Kudo A (2006) Photocatalytic hydrogen evolution on ZnS–$CuInS_2$–$AgInS_2$ solid solution photocatalysts with wide visible light absorption bands. Chem Mater 18:1969–1975
2. You D, Pan B, Jiang F, Zhou Y, Su W (2016) CdS nanoparticles/$CeO_2$ nanorods composite with high-efficiency visible-light-driven photocatalytic activity. Appl Surf Sci 363:154–160
3. Jin X, Chen F, Jia D, Cao Y, Duan H, Long M, Yang I (2019) Influences of synthetic conditions on the photocatalytic performance of ZnS/graphene composites. J Alloys Compd 780:299–305
4. Swain G, Sultana S, Parida K (2020) Constructing a novel surfactant-free $MoS_2$ nanosheet modified $MgIn_2S_4$ marigold microflower: an efficient visible-light driven 2D–2D p–n Heterojunction Photocatalyst Toward HER and pH regulated NRR. ACS Sustain Chem Eng 12:4848–4862
5. Peng S, An R, Li Y, Lu G, Li S (2012) Remarkable enhancement of photocatalytic hydrogen evolution over $Cd_{0.5}Zn_{0.5}S$ by bismuth-doping. Int J Hydrog Energy 37:1366–1374
6. Swain G, Sultana S, Moma J, Parida K (2018) Fabrication of hierarchical two-dimensional $MoS_2$ nanoflowers decorated upon cubic $CaIn_2S_4$ microflowers: facile approach to construct novel metal-Free p–n heterojunction semiconductors with superior charge separation efficiency. Inorg Chem 57(16):10059–10071
7. Lei Z, You W, Liu M, Zhou G, Takata T, Hara M, Domen K, Li C (2003) Photocatalytic water reduction under visible light on a novel $ZnIn_2S_4$ catalyst synthesized by hydrothermal method. Chem Commun 17:2142–2143
8. Yang G, Ding H, Chen D, Feng J, Hao Q, Zhu Y (2018) Construction of urchin-like $ZnIn_2S_4$–Au–$TiO_2$ heterostructure with enhanced activity for photocatalytic hydrogen evolution. Appl Catal B Environ 234:260–267
9. Li YX, Hou YL, Fu QY, Peng SQ, Hu YH (2017) Oriented growth of $ZnIn_2S_4$/$In(OH)_3$ heterojunction by a facile hydrothermal transformation for efficient photocatalytic $H_2$ production. Appl Catal B Environ 206:726–733
10. Swain G, Sultana S, Parida K (2019) One-Pot-architectured Au-nanodot-promoted $MoS_2$/$ZnIn_2S_4$: a novel p–n heterojunction photocatalyst for enhanced hydrogen production and phenol degradation. Inorg Chem 58(15):9941–9955
11. Shen S, Zhao L, Zhou Z, Guo L (2008) Enhanced photocatalytic hydrogen evolution over Cu-doped $ZnIn_2S_4$ under visible light irradiation. J Phys Chem C 112:16148–16155
12. Fan B, Chen ZH, Liu Q, Zhang ZG, Fang XM (2016) One-pot hydrothermal synthesis of Ni-doped $ZnIn_2S_4$ nanostructured film photoelectrodes with enhanced photoelectrochemical performance. Appl Surf Sci 370:252–259
13. Li Y, Wang J, Peng S, Liu G, Li S (2010) Photocatalytic hydrogen generation in the presence of glucose over ZnS-coated $ZnIn_2S_4$ under visible light irradiation. Int J Hydrog Energy 35:7116–7126
14. Zeng D, Xiao L, Ong W-J, Wu P, Zheng H, Chen Y, Peng D-L (2017) Hierarchical $ZnIn_2S_4$/$MoSe_2$ nanoarchitectures for efficient noble-metal-free photocatalytic hydrogen evolution under visible light. Chemsuschem 10:4624–4631
15. Xu B, He P, Liu H, Wang P, Zhou G, Wang X (2014) A 1D/2D helical CdS/$ZnIn_2S_4$ nano-heterostructure. Angew Chem Int Ed 53:2339–2343
16. Wang S, Guan BY, Lou XWD (2018) Construction of $ZnIn_2S_4$-$In_2O_3$ hierarchical tubular heterostructures for efficient $CO_2$ photoreduction. J Am Chem Soc 140:5037–5040
17. Yang J, Fu H, Yang DF, Gao WL, Cong RH, Yang T (2015) $ZnGa_{2-x}InxS_4$ ($0 \le x \le 0.4$) and $Zn_{1-2y}(CuGa)_yGa_{1.7}In_{0.3}S_4$ ($0.1 \le y \le 0.2$): optimize visible light photocatalytic $H_2$ evolution by fine modulation of band structures. Inorg Chem 54:2467–2473
18. Nanu M, Schooman J, Goossens (2005) Nanocomposite three-dimensional solar cells obtained by chemical spray deposition. Nano Lett 5:1716

19. Liu A, Yu C, Lin J, Sun G, Xu G, Huang Y, Liu Z, Tang C (2019) Construction of $CuInS_2$@ZIF-8 nanocomposites with enhanced photocatalytic activity and durability. Mater Res Bull 112:147–153
20. Aldakov D, Lefrancois A, Reiss P (2013) Ternary and quaternary metal chalcogenide nanocrystals: synthesis, properties and applications. J Phys Chem C 1:3756–3776
21. Guan Z, Pan J, Li Q, Li G, Yang J (2019) Boosting visible-light photocatalytic hydrogen evolution with an efficient $CuInS_2$/$ZnIn_2S_4$ 2D/2D heterojunction. ACS Sustain Chem. Eng 7:7736–7742
22. Han M, Yu Lu, Chen W, Wang W, Jia J (2016) Fabrication and photoelectrochemical characteristics of $In_2S_3$ nano-flower films on $TiO_2$ nanorods arrays. Appl Surf Sci 369:108–114
23. Song K, Zhu R, Tian F, Cao G, Ouyang F (2015) Effects of indium contents on photocatalytic performance of $ZnIn_2S_4$ for hydrogen evolution under visible light. J Solid State Chem 232:138–143
24. Shen SH, Zhao L, Guo LJ (2008) Cetyltrimethylammoniumbromide (CTAB)-assisted hydrothermal synthesis of $ZnIn_2S_4$ as an efficient visible-light-driven photocatalyst for hydrogen production. Int J Hydrog Energy 33:4501–4510
25. Feng C, Yang X, Sun Z, Xue J, Sun L, Wang J, He Z, Yu J (2019) Dual interfacial synergism in Au-Pd/$ZnIn_2S_4$ for promoting photocatalytic selective oxidation of aromatic alcohol. Appl Surf Sci 501:144018
26. Yuan D, Sun M, Tang S, Zhang Y, Wang Z, Qi J, Rao Y, Zhang Q (2020) All-solid-state $BiVO_4$/$ZnIn_2S_4$ Z-scheme composite with efficient charge separations for improved visible light photocatalytic organics degradation. Chin Chem Lett 31:547–550
27. Yue W, Han S, Peng R, Shen W, Geng H, Wu F, Tao S, Wang M (2010) $CuInS_2$ quantum dots synthesized by a solvothermal route and their application as effective electron acceptors for hybrid solar cells. J Mater Chem 20:7570–7578
28. Cao HY, Deng HM, Zhou WL, Tao JH, Chen LL, Huang L, Sun L, Yue FY, Yang PX, Chu JH (2015) Investigation of microstructural and optical properties of Cu(In, Al)$Se_2$ thin films with various copper content. J Alloy Compd 65:208–213
29. Tateishi I, Furukawa M, Katsumata H, Kaneco S (2019) The effect of Cu and Ga doped $ZnIn_2S_4$ under visible light on the high generation of $H_2$ production. ChemEngineering 3(4):79
30. Chen S, Li S, Xiong L, Wang G (2018) In-situ growth of $ZnIn_2S_4$ decorated on electrospun $TiO_2$ nanofibers with enhanced visible-light photocatalytic activity. Chem Phys Lett 706:68–75
31. Li Y, Han P, Hou Y, Peng S, Kuang X (2019) Oriented $Zn_mIn_2S_{m+3}$@$In_2S_3$ heterojunction with hierarchical structure for efficient photocatalytic hydrogen evolution. Appl Catal B: Environ 244:604–611
32. Xia Y, Li Q, Lv KL, Tang DG, Li M (2017) Superiority of graphene over carbon analogs for enhanced photocatalytic $H_2$-production activity of $ZnIn_2S_4$. Appl Catal B Environ 206:344–352
33. Zhang Z, Lin H, Zhang J, Wang F, Xie Y, Sheng X, Gu Y, Zhao H, Wang X (2018) In situ constructing interfacial contact $MoS_2$/$ZnIn_2S_4$ heterostructure for enhancing solar photocatalytic hydrogen evolution. Appl Catal B 233:112–119